JOURNAL OF CHEMICAL INFORMATION AND MODELING

Article

pubs.acs.org/jcim

REMD Simulations Reveal the Dynamic Profile and Mechanism of Action of Deleterious, Rescuing, and Stabilizing Perturbations to NBD1 from CFTR

Michael Zhenin, Efrat Noy, and Hanoch Senderowitz*

Department of Chemistry, Bar Ilan University, Ramat-Gan 52900, Israel

Supporting Information

ABSTRACT: Cystic Fibrosis (CF) is a lethal, genetic disease caused by mutations to the CFTR chloride channel. The most common CF causing mutation is the deletion of F508 from the first Nucleotide Binding Domain (F508del-NBD1). This mutation leads to a thermally unstable domain and a misfolded, nonfunctioning CFTR. Replica Exchange MD simulations were used to simulate seven NBD1 constructs including wt and F508del-NBD1 both alone and in the presence of known rescuing mutations as well as F508del-NBD1 in complex with a known small (ligand) stabilizer. Analyzing the resulting trajectories suggests that differences in the biochemical properties of the constructs result from local and coupled differences in their dynamic profiles. A comparative analysis of these profiles as well as of the resulting trajectories reveals how the different perturbations exert their deleterious, rescuing, and stabilizing effects on NBD1. These simulations may therefore be useful for the design and mechanism-of-action analysis of new NBD1 stabilizers.

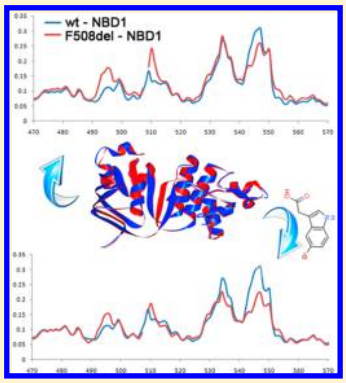

1. INTRODUCTION

Cystic Fibrosis (CF) is a genetic disease caused by mutations to the Cystic Fibrosis Transmembrane Conductance Regulator (CFTR) chloride channel.[1] CFTR is a member of the ABC (ATP-Binding Cassette) transporters family but has a unique functionality being the only ion channel in this group.[2] Nevertheless, CFTR architecture is similar to that of other ABC transporters, and its structure is comprised of two membrane spanning domains (MSDs) connected through four intracellular domains (ICDs) to two nucleotide binding domains (NBDs).[3,4] The role of the NBDs is to control the gating of the channel, which is located at the interface between the two MSDs through the binding of two and the hydrolysis of one ATP molecule(s).[3−8] Conformational changes in the NBDs brought about by the binding and hydrolysis of ATP are transmitted to the MSDs, likely via the ICDs.[9] In addition, CFTR features a unique intrinsically disordered R-region which is located at the sequence level between NBD1 and MSD2 and which must be phosphorylated to control channel gating.[10]

The most common mutation associated with CF is the deletion of F508 from the first of the two NBDs (F508del-NBD1).[11] Most of the mutant protein is incorrectly or incompletely folded and becomes targeted to endoplasmic reticulum-associated degradation (ERAD).[12] The few mutant chloride channels that escape degradation are eventually incorporated into the plasma membrane. However, these are thought to represent less than 5% of the level observed in cells expressing wt-CFTR and are characterized by an open probability about 15 folds lower than that of wt-CFTR[13] and a low membrane stability.[14−16] Studying the effect of the F508del mutation (as well as of other, less common mutations) on CFTR biosynthesis, structure and function is key to the development of new CF therapies.

The biosynthesis of CFTR is a complex process requiring the folding and assembly of multiple independent domains most likely in a combined cotranslational/post-translational manner.[17] This process has been extensively studied with a particular emphasis on the role of F508 and the impact of its deletion on the maturation of F508del-CFTR. Experimental evidence suggests that the F508del mutation reduces the folding efficiency and thermodynamic stability of NBD1 and also interferes with the interactions of NBD1 with other CFTR domains, in particular the ICDs and possibly NBD2.[18−28] Thibodeau et al.[25] have used multiple biochemical assays to evaluate the effect of a series of NBD1 mutations on the folding and maturation of the corresponding CFTR mutants. In particular it was found that the simultaneous introduction of three known suppressor mutations (G550E, R553Q, and R555K, Teem mutations) into the F508del background partially rescued the folding and the function of F508del-CFTR. In addition, these same three mutations produced a significant increase in the quantity of soluble F508del-NBD1 in two independent (bacterial and mammalian) systems. In another study, Clarke's group[29,30] found that the V510D mutation (and to a lesser extent the V510E mutation) promoted maturation of F508del-CFTR and increased the half-life of the mature protein at the cell surface to near wt-CFTR levels. This stabilizing effect was attributed to the formation of a salt bridge between the acidic residue at position

Received: May 25, 2015
Published: September 29, 2015

DOI: 10.1021/acs.jcim.5b00312
J. Chem. Inf. Model. 2015, 55, 2349−2364

510 and the Arginine residue at position 1070 which is located at the so-called coupling helix of ICL4.

Hunt, Brouillette, and co-workers have conducted isothermal[31] and thermal[24] denaturation studies of hNBD1 and demonstrated that the F508del mutation lowers the unfolding transition temperature of the wt protein by 6−7°, reduces its solubility, and promotes unfolding into an aggregation-prone state. They also demonstrated that suppressor mutations (including the Teem mutations and V510D) increase the in vitro solubility of F508del-NBD1, protect it from the intensified unfolding and aggregation, and elevate its unfolding transition temperature.

Taken together, these observations suggest that the F508del and suppressor mutations impact the maturation and function of F508del-CFTR by altering inherent properties of NBD1, independently of the exact nature of the chaperone system. Recent studies from the Thomas[27] and Lukacs[28] laboratories demonstrated that restoring wt-like behavior to F508del-CFTR requires the simultaneous stabilization of F508del-NBD1 as well as its interactions with ICL4. Interestingly, both effects could be mediated through F508del-NBD1 itself (e.g., through the synergic combination of V510D and the 3S mutations, F494N, Q637R, F429S).[28] Somewhat in contrast with this proposition, He et al. have demonstrated that restoring the thermal stability of NBD1 is sufficient to promote F508del-CFTR maturation.[32] Irrespective of the particular details, it is clear however that NBD1 is a viable target for the rescuing of the full protein, potentially through (a combination of) small ligand binding.

Multiple small ligands have been shown to either correct or potentiate various CFTR mutants. In particular, Vertex's Kalydeco (VX-770) potentiates multiple CFTR mutants including G551D (for which it was FDA-approved) but also e.g. S549N, G551S, G1244E, and F508del.[33,34] F508del-CFTR could be corrected by other compounds from the Vertex pipeline, for example, VX-809 and VX-661. However, none of these ligands is expected to bind NBD1. There is evidence suggesting that VX-809 corrects F508del-CFTR by interacting with TMD1,[35] whereas the binding site of VX-770 is to date unknown.

Ligands directly binding to NBD1 were discovered by SGX Pharmaceuticals using high throughput crystallography experiments. Importantly, at least two of these ligands were found to stabilize F508del-NBD1 by 1.4 and 2.4 °C.[32]

In light of the profound effect of the F508del mutation on CFTR function and stability it is interesting to note that a comparative analysis of a collection of crystal structures of wt and F508del-NBD1 from human and murine CFTR[21,36−39] suggests that the ground states of the two proteins are similar, with consistent differences primarily localized to the F508 region[27,36,40] (Figure 1). In contrast, NMR studies of the murine forms of the two proteins are consistent with local and nonlocal differences in the dynamic profiles of their solution structures, differences that influence the chemical shifts of residues located as far as 30−40 Å away from the location of F508.[41] It is likely that ground state similarity and differences in dynamic profiles also exist for other NBD1 mutants.

The dynamic profiles of wt and F508del-NBD1 have also been studied using molecular dynamics (MD) simulations, albeit with inconsistent results. Thus, Wieczorek and Zielenkiewicz[42] performed a single 20 ns MD simulation of wt and F508del-NBD1 and based on RMSD plots, principal component analysis of the resulting trajectories and analysis of

Figure 1. Superposition of wt and F508del-NBD1. Superposition of wt (blue, 2PZE) and F508del (red, 2PZF) RIdel, REdel-NBD1. The two proteins overlap with a backbone RMSD of 0.61 Å. F508 is depicted in a stick representation.

the accessible surface areas concluded that the mutant protein has an enhanced conformational freedom with respect to the wt, which results in exposure of hydrophobic surface area to the solvent. In contrast Bisignano and Moran[43] have performed a series of shorter (5 ns) simulations on the two proteins and by analyzing the resulting Root Mean Squared Fluctuations (RMSF) profiles concluded that no appreciable differences in their dynamic profile are apparent. Aleksandrov et al. performed discrete MD (DMD) simulations to study the effect of the (modeled) regulatory insertion (RI) on the dynamics of wt and F508del-NBD1 and found that the removal of this segment reduces the fluctuations of the mutant to wt level. Finally, Proctor et al. have studied allosteric coupling in NBD1 using a coupled dynamics network approach and identified S492 as a key mediator of RI-induced fluctuations in F508del and I507del-NBD1.[44]

In order to provide new insight into the dynamics of wt and mutant NBD1 as well as into the effect on protein dynamics of a known NBD1 stabilizer we have subjected a series of NBD1 constructs (wt, V510D, 3M, F508del, F508del/V510D, F508del/3M, and F508del/BIA, a known NBD1 stabilizer[32]) to lengthy Replica Exchange MD (REMD) simulations. We based our simulations on the most recently solved crystal structures of human NBD1, namely 2PZE (wt) and 2PZF (F508del). These were solved after the removal of the entire regulatory insertion (RI, residues 405−436) but with no other solubilizing mutations. The removal of the RI was shown to restore maturation and improve the stability and function of F508del-CFTR,[45] yet the thermal stability of RIdel/F508del-NBD1 was still found to be lower than that of the corresponding RIdel-NBD1 construct by ∼6−7 °C in agreement with similar differences observed for other NBD1 constructs.[24] Importantly, the removal of the RI improves the stability of NBD1 rendering it more amenable to biochemical assays. Thus, a reasonably large volume of experimental data exists for RIdel constructs[24] which is important for the validation of our computational approach. Finally, due to the disordered nature of the RI and the concomitant absence of electron densities for this domain in all human NBD1 crystal structures solved to date, its inclusion in the simulated system may lead to potential large uncertainties.

RMSF profiles obtained from our REMD simulations show that the fluctuations of a few segments of F508del-NBD1 not only in the vicinity of the F508del mutation but also in other

DOI: 10.1021/acs.jcim.5b00312
J. Chem. Inf. Model. 2015, 55, 2349−2364

parts of the protein are consistently higher than those of wt-NBD1 in agreement with its lower thermal stability.[24,31] We provide structural interpretation for the high fluctuations of the above-mentioned segments based on the static crystal structures and on their dynamic coupling revealed by the REMD trajectory. In addition, the RMSF profiles provide insight into the mechanism by which the F508del mutation exerts its deleterious effect on NBD1, insight which is in line with available experimental data. We performed similar simulations on NBD1 and its F508del mutant in the presence of V510D and the Teem mutations (G550E, R553Q, and R555K), providing preliminary insight into their rescuing mechanism. In addition, we present here REMD simulations of the F508del mutant in the presence of a known stabilizer identified by SGX (BIA). We demonstrate that the presence of this ligand reduces the fluctuations of F508del-NBD1, in particular in regions where this domain interacts with other domains of the full length protein (ICL3 and ICL4), thereby providing structural interpretation which can help in elucidating its stabilizing mechanism. Finally, we demonstrate a significant correlation between RMSF profiles and thermal stability data across the seven NBD1 constructs considered in this work.

2. METHODS

2.1. System Preparation. Simulations were performed for wt and F508del human RIdel, REdel-NBD1, comprising residues 387−646 (excluding a deletion of residues 405−436) with no additional solubilizing mutations (PDB entries 2PZE, 1.7 Å resolution and 2PZF, 2.0 Å resolution, respectively). Both structures were solved in the presence of ATP and a Mg^{2+} ion.

Prior to simulations, proteins were prepared using the Prepare Protein protocol in Discovery studio.[46] This protocol inserts missing atoms in incomplete residues, models missing loop regions (in 2PZE: Q637-P638, in 2PZF: E402-E403 and Q637-P638), and sets the protonation state of titratable residues based on predicted pK_a values.

ATP parameters for the OPLS/AA force field were parsed from the OPLS/AA 2001 force field parameters in Schrodinger[47] and modified to Gromacs topology file by Perl scripting. The parameters for the Mg^{2+} ion are included in the GROMACS implementation of this force field.

V510D and the Teem mutations were introduced into wt and F508del backgrounds by mutating the relevant residues in 2PZE and 2PZF, respectively, using Discovery Studio.[46] Mutated residues and their 5 Å neighboring residues were optimized using the side-chain refinement protocol in Discovery Studio.[46]

Investigating the effect of a known NBD1 stabilizer on F508del-NBD1 (BIA) was performed by simulating 2PZF (F508del-NBD1) in the presence of this ligand, using coordinates provided by SGX Pharmaceuticals. For consistency, the original SGX structure and 2PZF were superposed, and the coordinates of the ligand were copied from the former to the latter. Similar to ATP, force field parameters for this ligand were parsed from the OPLS/AA 2001 force field parameters in Schrodinger.

2.2. REMD Simulations. All REMD simulations were performed with the Gromacs Molecular Dynamics package version 4.5.5[48,49] using the OPLS/AA force field.[50] The proteins were submerged in TIP4P water in rhombic dodecahedral boxes with an additional 10 Å extension along each axis of the protein. Ions were added to the solution to make the system electrically neutral. Structures were energy-minimized with the steepest descent algorithm until the convergence criterion of a maximum force smaller than 10.0 kJ/mol/nm was met.

Following minimization, each replica (see below for description of the replicas) was equilibrated for 100 ps under NVT conditions. At this stage the solvent and the solute were independently coupled to a bath of the respective replica's temperature with relaxation time of 0.1 ps by means of the V-rescale algorithm.[51] Next, each replica was equilibrated for an additional 100 ps under NPT conditions using the Brendsen pressure coupling with a coupling time of 1.0 ps and a compressibility constant of 4.5×10^{-5} bar^{-1}. Finally, REMD production phase simulations were carried out under NPT conditions with the leapfrog algorithm[52] using a 2 fs time step. Long-range electrostatic interactions were computed using Particle Mesh Ewald (PME) electrostatics.[53,54] The relative strength of the Ewald-shifted direct potential at the cutoff was 1.0×10^{-5}. The maximum grid spacing for the fast Fourier transform (PME) was set to 1.2 Å. Cutoffs for van der Waals and Coulomb interactions were set to 10 Å. Periodic boundary conditions were applied in all simulations. The LINCS algorithm[55] was used to constrain bond lengths.

Each of the seven constructs considered in this work was simulated three times, each time starting from a different random seed number. Each REMD simulation consisted of 32 replicas covering a temperature range of 300 K (26.85 °C) to 349.38 K (76.23 °C) (which is above the Tm of all constructs) with each replica running for 10 ns. Thus, each construct was simulated for a total of 960 ns (32 replicas × 10 ns × 3 times). In all the simulations, the temperature range was selected so as to give the same acceptance probability between all adjacent pairs over the entire temperature range based on known energy distributions of solvated proteins.[56]

2.3. Solvent Accessible Surface Area. Solvent accessible surface area was calculated using the double cube lattice method as implemented in Gromacs.[57] Differences in SASA values were calculated while taking into account standard deviations and consequently reflect minimal differences. This approach allows focusing on the most significantly different regions.

2.4. Data Analysis. All analyses were performed on the lowest temperature (ground state) replicas. The dynamic behavior of the proteins was evaluated by calculating a RMSF profile for each trajectory and comparing the effect of perturbation (either mutation or the presence of BIA) on the profiles. Residues defined to be consistently different in the unperturbed and the perturbed constructs are those having RMSF values consistently higher (or lower) across all simulation repeats. Regions defined to be consistently different in the unperturbed and the perturbed construct are those having at least three consecutive different residues. Prior to calculation, all structures were superposed on the corresponding crystal structure using all backbone atoms.

2.4.1. Normalized Covariance Matrix. To unveil the dynamic coupling between structurally distant regions, normalized covariance matrices of C_α coordinates[58] were calculated for wt and for each of the perturbed NBD1 constructs using eq 1. The normalized covariance, also called correlation coefficient, is a measure of the linear dependence between the movements of two C_α atoms and is bound between +1 (perfect correlation) and −1 (perfect anticorrelation).

DOI: 10.1021/acs.jcim.5b00312
J. Chem. Inf. Model. 2015, 55, 2349−2364

$$N_{\mathrm{cov}(X,Y)}\frac{\sum((X_i-\langle X\rangle)\cdot(Y_i-\langle Y\rangle))}{\sqrt{\sum(X_i-\langle X\rangle)^2\cdot\sum(Y_i-\langle Y\rangle)^2}} \quad (1)$$

In eq 1, $\langle X\rangle$ and $\langle Y\rangle$ are averages of coordinates of specific C_α atoms calculated over snapshots taken from the simulation trajectory. X_i and Y_i are coordinates of these C_α atoms in the individual snapshots. Covariance matrices were calculated based on structures superposed as described above.

2.4.2. Conformational Clustering. Conformational clustering was used to compare the potential energy surfaces (PESs) sampled by the different constructs. For this purpose, 100 representative snapshots were taken from each trajectory for a total of 100 snapshots × 3 repeats × 7 structures = 2100 conformations. These were superposed on a single reference structure (the crystal structure of wt-NBD1) using backbone atoms and subjected to average linkage hierarchical clustering using Schrodinger's Maestro.[47] Following clustering, the optimal number of clusters according to the Kelley criterion was found to be 36. However, under this clustering scheme ~90% of all conformers resided in a single cluster. In order to allow for a more meaningful analysis the number of clusters was increased to 40, and the resulting clusters were examined for their conformational memberships. A similar procedure using the same structures was applied to ATP to compare its binding mode in the different constructs. In this case, the optimal number of clusters was found to be 99.

2.4.3. Pocket Analysis. A representative trajectory of F508del-NBD1 was subjected to a pocket finding algorithm using MDpocket as implemented in the fpocket software.[59]

3. RESULTS

System sizes and acceptance ratios between all neighboring replicas in all constructs are presented in Table S1. Graphs describing the round trip of the lowest energy replicas as well as the replicas contributing to the lowest temperature trajectory for each constructs are provided in Figures S1–S7.

3.1. REMD Simulations of wt and F508del-NBD1. Three independent REMD simulations were performed on wt and F508del-NBD1 (a total of six simulations). The resulting trajectories were assessed in terms of their RMSD and RMSF profiles. Both measures were found to be consistent over the three trajectories of each construct (Figure S8 in the Supporting Information and Figure 2).

REMD-generated RMSF profiles clearly show that the fluctuations of F508del-NBD1 are overall higher than those of wt-NBD1, in agreement with its lower thermal stability.[24] Furthermore, 28% (61 residues) of the residues were found to have consistently higher RMSF values in F508del compared with wt, whereas only two residues showed consistently higher RMSF values in the wt. Regions consisting of at least three consecutive residues for which F508del RMSF values were found to be consistently higher than those of wt are found in the vicinity of F508, at the α subdomain (501–505, 510–512, 551–557), and at the interface between the α/β and α subdomains (491–497, 564–566). Consistent differences were also observed for residues distant from F508, at the α/β-subdomain (583–588, 593–595; see Figure 2B). The differences found for residues 501–505 and 510–512 are in agreement with H/D exchange data.[40]

The original X-ray structures provide a structural interpretation for a few of the regions in the close vicinity of F508. Upon deletion of F508, V510 changes its "inward facing"

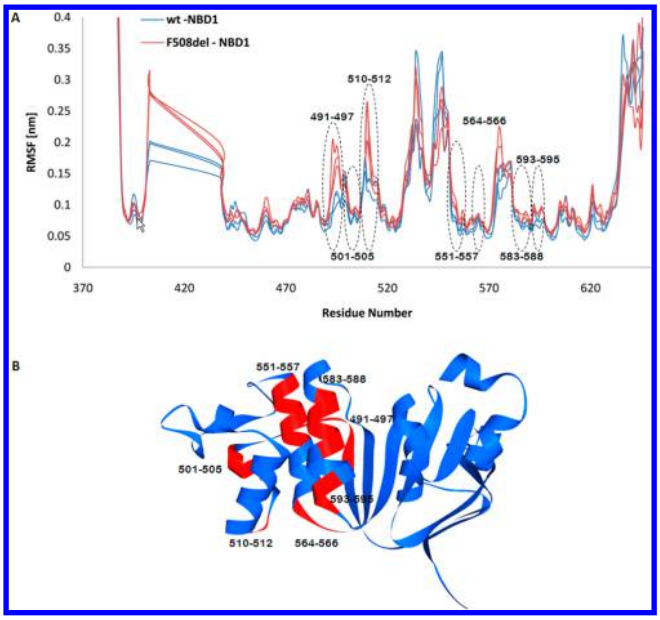

Figure 2. RMSF profiles of wt and F508del-NBD1 constructs from REMD simulations. (A) RMSF profiles for wt (blue, three repeats) and F508del (red, three repeats) RIdel, REdel-NBD1 constructs obtained from REMD simulations. Tm values: 57.7 and 51.5 °C for wt and F508del-NBD1, respectively. Residues 405–436 correspond to the missing RI region. Regions (consecutive sets of at least 3 residues) for which F508del RMSF values are consistently higher than those of the wt are circled (see the Methods section for the meaning of consistency in this context). (B) Differences between wt and F508del-NBD1 mapped on the NBD1 structure. The circled regions in (A) are colored red.

orientation and becomes exposed to solution,[40] thereby increasing the flexibility of the 510–512 region. The increased exposure and dynamics of the 510–512 loop could promote aberrant intermolecular interactions[40] or expose hydrophobic surface area to solution, thereby increasing the aggregation tendency of F508del-NBD1 in accord with experimental observations.[24,60] Moreover, a π–π interaction between W496 and F508 is lost in the mutant (the side chain of W496 adopts a different orientation in the mutant than in the wt protein), causing the 491–497 region, which forms a linker between α and α/β subdomains of NBD1 to become more flexible. ATP binds to the NBD in the vicinity of this region, and this may explain experimental results showing weaker ATP binding by F508del-NBD1.[61,62]

Next we analyzed the simulation trajectories for dynamic coupling between different regions by computing normalized covariance matrices.[58] Normalized covariance matrices were generated for each of the three wt and three F508del simulations and averaged to reproduce a single matrix for each construct (see Figures 3A and 3B for wt and F508del-NBD1, respectively). Overall, 608 and 648 correlations with values >0.6 were identified for wt and F508del-NBD1, respectively, demonstrating the existence of a complex network of allosteric interactions which spread across the entire protein.

This analysis revealed that the large fluctuations in positions 501–505 and 491–497, in close vicinity to the deleted 508 residue, are correlated with each other (red circle in Figure 3). Furthermore, positions 564–566, located at the interface between the α and β subdomains, and position 487, located at the interface between the β and α/β subdomains are also correlated with each other (black circle in Figure 3). These

DOI: 10.1021/acs.jcim.5b00312
J. Chem. Inf. Model. 2015, 55, 2349–2364

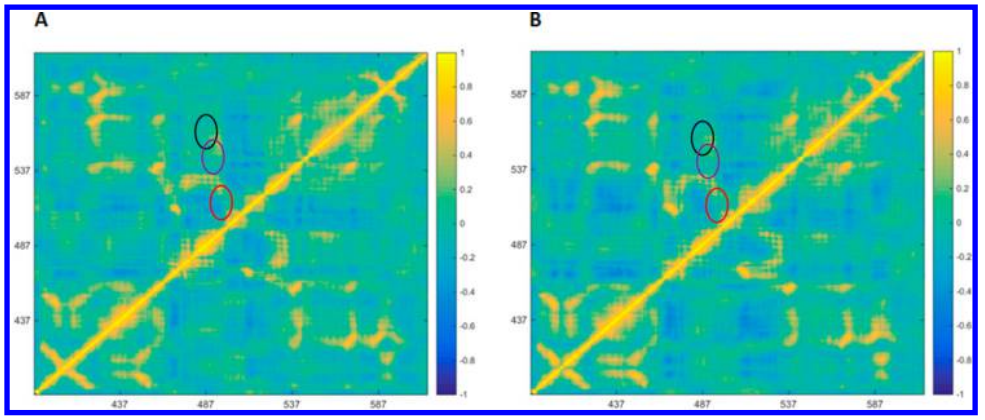

Figure 3. Correlation matrices for wt and F508del-NBD1. (A) Averaged covariance matrix indicating the degree of linear dependence between the movements of C_α atoms for wt-NBD1. Coloring scheme ranges from yellow (perfect correlation) to blue (perfect anticorrelation). (B) Averaged covariance matrix for F508del-NBD1. Circles highlight specific regions discussed in the text.

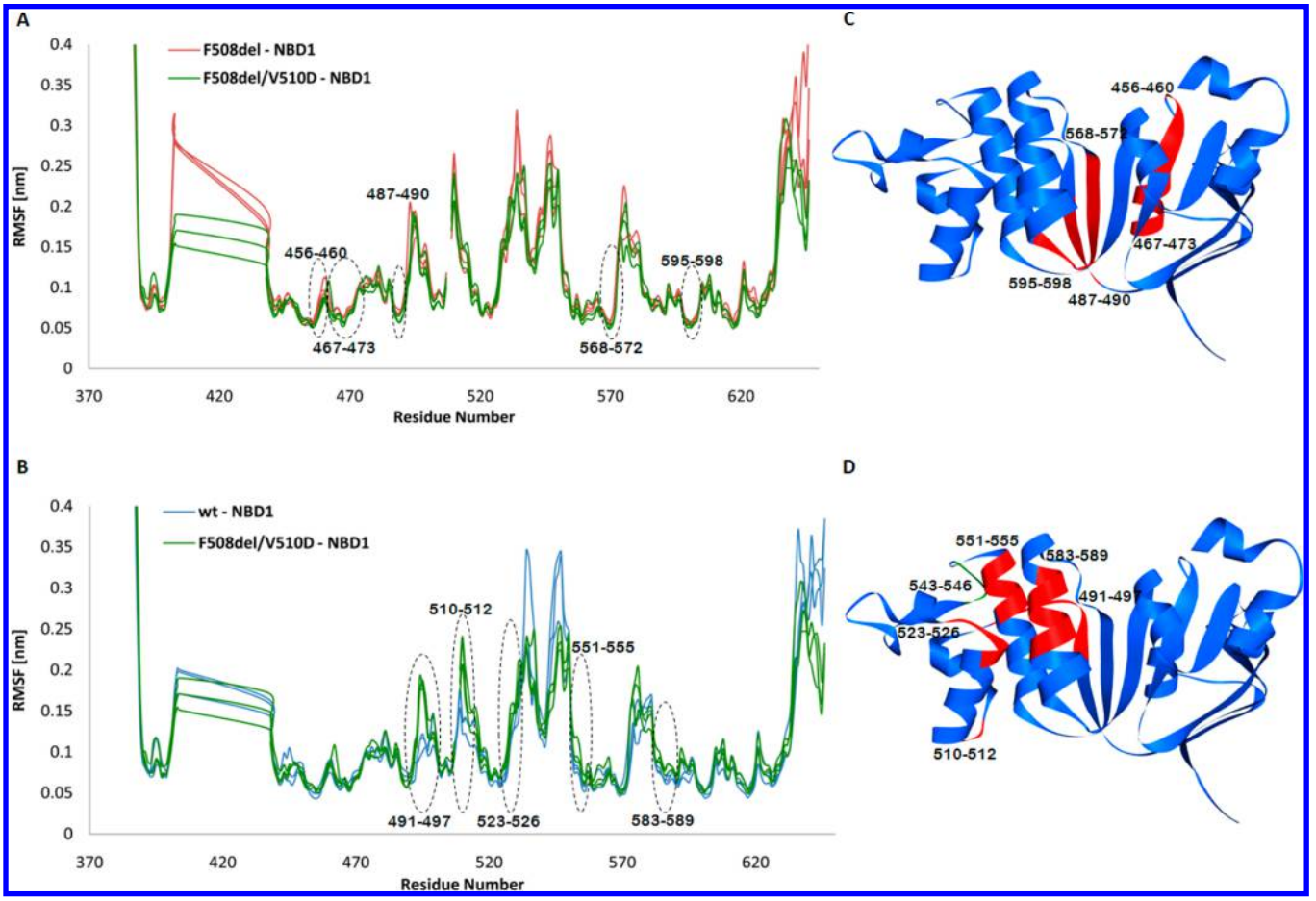

Figure 4. A comparison between RMSF profiles of wt, F508del, and F508del/V510D-NBD1 constructs from REMD simulations. (A) REMD-derived RMSF profiles for F508del (red, three repeats) and F508del/V510D-NBD1 (green, three repeats). Tm values: 51.5 and 53.0 °C for F508del and F508del/V510D-NBD1, respectively. Regions of consistent differences between the profiles are circled. (B) REMD-derived RMSF profiles for wt (blue, three repeats) and F508del/V510D-NBD1 (green, three repeats). Tm values: 57.7 and 53.0 °C for wt and F508del/V510D-NBD1, respectively. Regions of consistent differences between the profiles are circled. (C) Differences between F508del-NBD1 and F508del/V510D-NBD1 mapped on the NBD1 structure. Regions consisting of at least three consecutive residues for which F508del RMSF values are consistently higher than those of F508del/V510D are colored in red. (D) Differences between wt and F508del/V510D-NBD1 mapped on the NBD1 structure. Regions consisting of at least three consecutive residues for which F508del/V510D RMSF values are consistently higher than those of wt are colored in red. Regions consisting of at least three consecutive residues for which wt RMSF values are consistently higher than those of F508del/V510D are colored in green.

dynamic correlations were observed in the simulations of both wt and F508del proteins. In contrast, segment 491−497 is correlated with segment 542−544 only in the F508del structure (magenta circle in Figure 3). This correlation is likely the result

DOI: 10.1021/acs.jcim.5b00312
J. Chem. Inf. Model. 2015, 55, 2349−2364

of the conformational change experienced by W496 in the mutant protein which brings it into close contact with E543. Indeed a hydrogen bond between the carboxyl group of E543 and the indole hydrogen of W496 is present, on average, in 34% of the simulation of the mutant protein, whereas it is completely lacking in the wt. The presence of this hydrogen bond is also reflected in the higher RMSF value of the 543−545 region in the wt. Interestingly, E543 was shown to interact with ICL3 and ICL4 in wt-CFTR.[63] We therefore hypothesize that the W496-E543 hydrogen bond formed in F508del-NBD1 prevents E543 from forming critical contacts with the ICLs, contributing to the improper folding of F508del-CFTR.

We have also calculated the sum of the averaged solvent accessible surface area (SASA) and the sum of the averaged hydrophobic SASA over all trajectories and found them to be 13,129 ± 26 Å^2 and 6,626 ± 9 Å^2 for wt and 13,157 ± 65 Å^2 and 6,573 ± 26 Å^2 for F508del-NBD1. These values are not significantly different from each other. Several hydrophobic residues were found to significantly increase their exposed surface area in the mutant including W496 (126 ± 4 Å^2 and 154 ± 1 Å^2 for wt and F508del-NBD1, respectively), V510 (69 ± 2 Å^2 and 131 ± 6 Å^2 for wt and F508del-NBD1, respectively), R560 (46 ± 5 Å^2 and 96 ± 3 Å^2 for wt and F508del-NBD1, respectively), and M498 (66 ± 1 Å^2 and 85 ± 4 Å^2 for wt and F508del-NBD1, respectively; see Table S2). Such changes were previously reported for the first two residues.[40,43]). In contrast, several hydrophilic residues were found to significantly decrease their exposed surface area, in particular E543 (129 ± 1 Å^2 and 114 ± 6 Å^2 for wt and F508del-NBD1, respectively) and S511 (82 ± 1 Å^2 and 70 ± 1 Å^2 for wt and F508del-NBD1, respectively). Local exposure of hydrophobic surface area in the mutant may explain the increased aggregation tendency of F508del-NBD1.[24,40,60]

3.2. REMD Simulations of V510D and F508del/V510D-NBD1. REMD simulations were also performed on two constructs containing the rescuing mutation V510D (V510D-NBD1 and F508del/V510D-NBD1). This mutation increases the folding efficiency of F508del-CFTR and the half-life of mature F508del-CFTR at the cell surface, probably through formation of a salt bridge with R1070 in TMD2.[28,30] In addition, V510D stabilizes both wt and F508del-NBD1, increasing their melting temperatures from 57.7 to 60.2 °C and from 51.5 to 53.0 °C, respectively.[24] As before, REMD simulations of both constructs were repeated three times, and the resulting trajectories were found to be reproducible (see Figure S9 and Figure 4).

A possible explanation to the stabilizing/rescuing effect which V510D exerts on NBD1 can be provided by examining snapshots from the simulations. In wt-NBD1 the aspartic acid is facing inward and consequently is involved in salt bridges mainly with R516 (73% of the time) and occasionally with R487 (18% of the time). The salt bridge with R487 stabilizes the interaction between the α-subdomain and the α/β-subdomain. In F508del/V510D-NBD1 the aspartic acid is facing the solution, and consequently these salt bridges are less prevalent. In addition, stabilization and prevention of aggregation may result from exposure to the solution of a hydrophilic (D) rather than a hydrophobic (V) residue as well as from a small increase in the SASA of the hydrophilic residue Q493 (from 90 ± 8 Å^2 in F508del-NBD1 to 104 ± 3 Å^2 in F508del/V510D-NBD1). The difference between the suggested stabilization mechanisms of wt and F508del-NBD1 by V510D is in line with the different shifts in Tm induced by the mutation (+2.5 °C and +1.5 °C for the wt and mutant protein, respectively).

Another explanation to the favorable effect of V510D can be provided by comparing the REMD-generated RMSF profiles of F508del and F508del/V510D-NBD1 (Figure 4A). V510D leads to a consistent attenuation of the F508del-NBD1 fluctuation profile in several regions (456−460, 467−473, 487−490, 568−572, 595−598; see Figures 4A, C), most of which are located within the α/β subdomain. Moreover, based on the CFTR model recently published by Mornon et al.[64] regions 467−473 and 487−490 are in the vicinity of ICL4. Reduced fluctuations in these regions may therefore stabilize the NBD1-ICL4 interface which is critical for proper protein folding.

Another instructive comparison could be made between the RMSF profiles of wt and F508del/V510D-NBD1 (Figure 4B and 4D). In the presence of V510D, the RMSF values of F508del are still overall higher than those of the wt protein, again in agreement with its lower thermal stability (57.7 and 53.0 °C for wt and F508del/V510D-NBD1, respectively).[24] However, the differences in fluctuations are smaller than those observed between wt and F508del in accord with the rescuing effect of V510D. Accordingly, several of the regions found to consistently fluctuate to a higher degree in F508del compared to wt-NBD1 disappear upon introducing the V510D mutation (501−505, 564−566, and 593−595), while only a single new region emerges (523−526). Consequently, 37 residues (17%) have consistently higher RMSF values in F508del/V510D than in wt compared to 28% in F508del-NBD1. Moreover, nine residues (4%) show the opposite effect, having consistently higher fluctuations in wt compared with F508del/V510D. Regions consisting of at least three consecutive residues for which F508del/V510D RMSF values are consistently higher than those of wt were found in the vicinity of F508, at the α-subdomain (residues, 510−512, 523−526 and 551−555) and at the interface between the α/β and α subdomains (residues 491−497). Differences were also observed for residues located away from F508, at the α/β subdomain (residue 583−589). The single region with higher fluctuations in wt compared to the mutant (residues 543−546) is located at the α-subdomain. The attenuation of the fluctuations in the mutant protein in this region results from formation of a hydrogen bond between W496, which maintains the same conformation in F508del/V510D-NBD1 as in F508del-NBD1 and E543. This hydrogen bond is maintained throughout 27% of the simulation.

As before, three normalized covariance matrices of each construct were calculated and averaged to analyze dynamic coupling in simulation trajectories between different segments. The resulting matrix of F508del/V510D-NBD1 is highly similar to that of F508del-NBD1 (and is therefore not shown), including the H-bond induced E543-W496 correlation which was not observed in the wt. Thus, we hypothesize that V510D does not rescue F508del-CFTR by reconstituting important contacts between E543 and ICL3/4 but rather by using an alternative mechanism (e.g., formation of a salt bridge with R1070 as discussed above).

3.3. REMD Simulations of G550E/R553Q/R555K (3M) and F508del/3M-NBD1. The simultaneous introduction of three known suppressor mutations, G550E, R553Q, and R555K (3M, Teem mutations), significantly increases the solubility[25] and thermal stability of wt and F508del-NBD1 (a raise in Tm from 57.7 to 61.7 °C and from 51.5 to 55.7 °C for wt and F508del-NBD1, respectively[24]). This stabilization is translated

DOI: 10.1021/acs.jcim.5b00312
J. Chem. Inf. Model. 2015, 55, 2349−2364

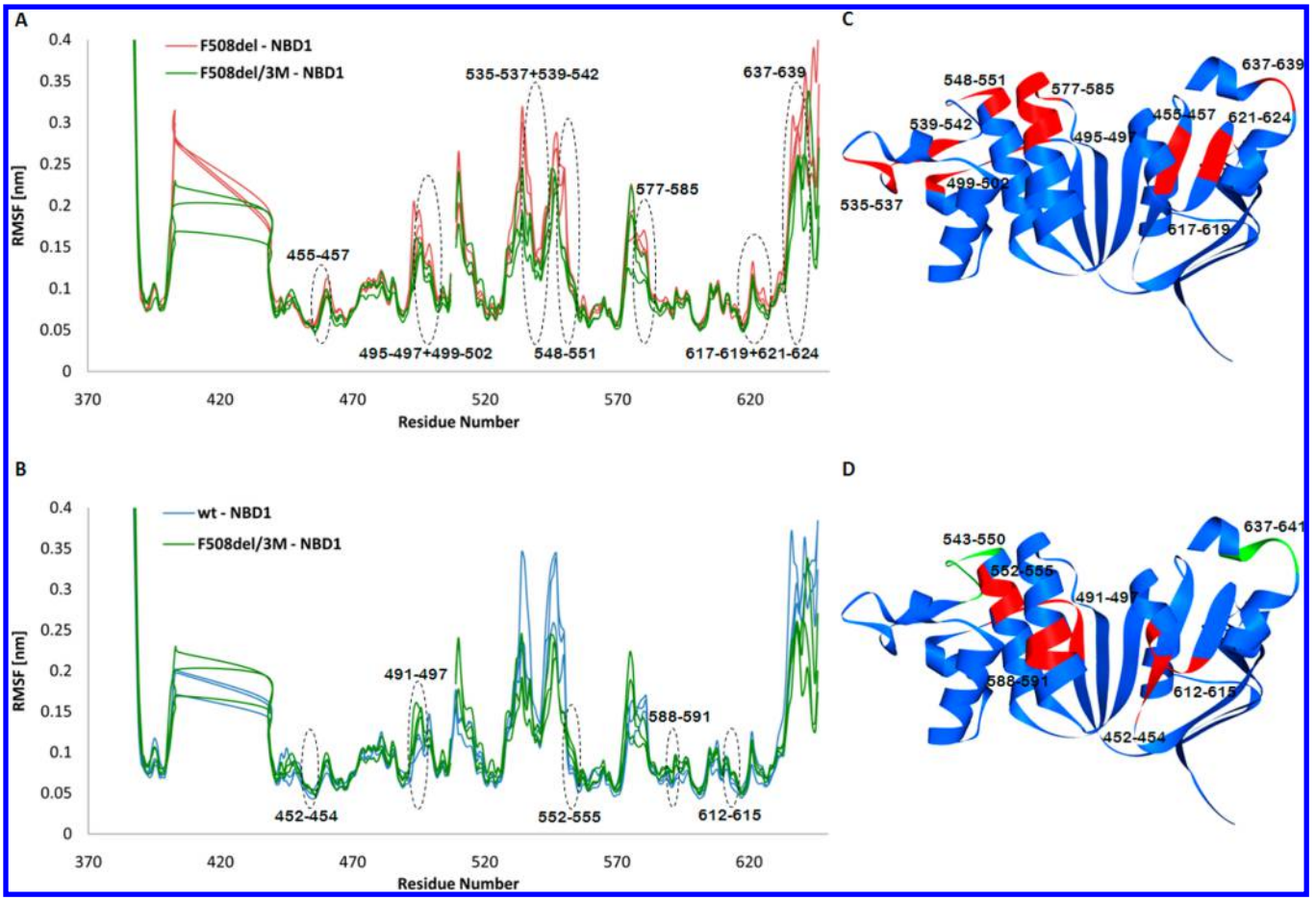

Figure 5. A comparison between RMSF profiles of wt, F508del, and F508del/3M-NBD1 constructs from REMD simulations. (A) REMD-derived RMSF profiles for F508del (red, three repeats) and F508del/3M-NBD1 (green, three repeats). Tm values: 51.5 and 55.7 °C for F508del and F508del/3M-NBD1, respectively (B) REMD-derived RMSF profiles for wt (blue, three repeats) and F508del/3M-NBD1 (green, three repeats). Tm values: 57.7 and 55.7 °C for wt and F508del/3M-NBD1, respectively. (C) Differences between F508del-NBD1 and F508del/3M-NBD1 mapped on the NBD1 structure. Regions consisting of at least three consecutive residues for which F508del RMSF values are consistently higher than those of F508del/3M are colored in red. (D) Differences between wt and F508del/3M-NBD1 mapped on the NBD1 structure. Regions consisting of at least three consecutive residues for which F508del/3M RMSF values are consistently higher than those of wt are colored in red. Regions consisting of at least three consecutive residues for which wt RMSF values are consistently higher than those of F508del/3M are colored in green.

into a partial rescue of both maturation and function of F508del-CFTR.[25,27,28]

REMD simulations of both 3M and F508del/3M-NBD1 were repeated three times and as above provided consistent results (Figure S10 and Figure 5). Snapshots taken from the resulting trajectories provide structural interpretation for the stabilizing effect of the Teem mutations on wt and F508del. Position 555, whether occupied by arginine[27] or lysine, is involved in a salt bridge with D529 in wt, 3M, F508del, and F508del/3M-NBD1. The R555K mutation seems to stabilize NBD1 since exposed salt bridges, as the one between R555/K555 and D529, energetically favor lysine over arginine.[65] Position 550 is exposed to solution in all constructs, and its mutation to Glutamic acid likely increases NBD1 solubility, decreases its aggregation propensity, and consequently increases its stability. The effect of R553Q is less obvious. This is in line with a similar mutation, R553M, which was reported to be less effective than R555K and G550E in promoting F508del-CFTR maturation.[26] We do not observe any mutual effect of the three mutations, in agreement with experimental results.[66−68]

In addition, a comparison of REMD-generated RMSF profiles between F508del and F508del/3M-NBD1 (Figure 5A and 5C) clearly demonstrates that the introduction of the Teem mutations strongly attenuates the fluctuations of multiple regions in NBD1 (455−457, 495−497, 499−502, 535−537, 539−542, 548−551, 577−585, 617−619, 621−624, 637−639) roughly bringing the RMSF profile to the level of wt (Figure 5B). The degree of attenuation obtained by the Teem mutations exceeds that obtained by V510D in agreement with their larger effect on protein stability (the Teem mutations increase the Tm of wt and F508del-NBD1 by 4 and 4.2 °C, respectively, whereas V510D increases the Tm of wt and F508del-NBD1 by 2.5 and 1.5 °C, respectively). Moreover, in contrast with the effect of V510D, the Teem mutations affect both α and α/β subdomains within NBD1. Two of the above-mentioned regions (499−502 and 539−542) are in the vicinity of ICL3, based on Mornon's model.[64] Reduced fluctuations in these regions may therefore stabilize the critical NBD1-ICL3 interface. Some of the regions affected by the Teem mutations are intercorrelated (455−457 with 617−619, 495−497 with 539−542, 499−502 with 539−542; see red circles in Figure 6) stressing once more the high allostericity of NBD1.

DOI: 10.1021/acs.jcim.5b00312
J. Chem. Inf. Model. 2015, 55, 2349−2364

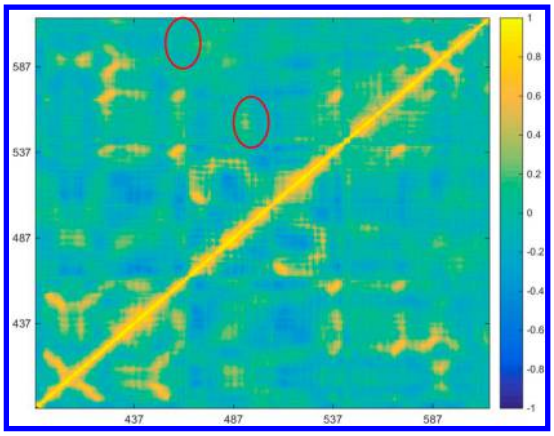

Figure 6. Correlation matrices for F508del/3M-NBD1. Averaged covariance matrix indicating the degree of linear dependence between the movements of C_α atoms for F508del/3M-NBD1. Coloring scheme ranges from yellow (perfect correlation) to blue (perfect anticorrelation). Circles highlight regions discussed in the text.

A comparison between the RMSF profiles of wt and F508del/3M-NBD1 is provided in Figures 5B and 5D and demonstrates consistently higher fluctuations in the mutant for 14% of the residues and higher fluctuations in wt for 7% of the residues. These percentages are in agreement with a significant stabilization of ~4 °C by the Teem mutations.[24] Contiguous regions for which F508del/3M RMSF values are higher than those of wt are found in the vicinity of F508, at the α subdomain (552−555), at the interface between the α/β and α subdomains (residues 491−497), and also at distant regions, namely, the α/β subdomain (452−454, 588−591, and 612−615; see Figure 5D). More than half of the regions showing consistent differences in fluctuations between wt and F508del-NBD1 disappear upon including the Teem mutations (501−505, 510−512, 564−566, and 593−595), while a few others emerge (452−454 and 612−615 both in the α/β−subdomain). Interestingly, the newly emerging regions were found to be dynamically coupled (Figure 6).

Three regions, 491−497, 552−555, and part of 583−588, show consistently higher fluctuations in all F508del-containing constructs in comparison with wt.

3.4. REMD Simulations of F508del-NBD1 in Complex with BIA (F508del/BIA-NBD1). REMD simulations were also performed for the F508del construct in complex with the known NBD1 stabilizer BIA (Figure 7). This ligand was found to increase the stability of F508del-NBD1 by 1.4 °C.[32]

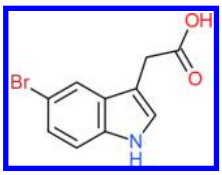

Figure 7. SGX Pharmaceuticals ligand, BIA, 5-bromoindole-3-acetic acid.

Three repeats of REMD simulations of the BIA/F508del-NBD1 complex provided trajectories with small RMSD values relative to the initial crystal structure and consistent RMSF profiles (see Figure S11 and Figure 8). The ligand remained tightly bound to the protein throughout all the simulations.

Examination of the trajectories provides an interpretation for the stabilization effect BIA exerts on F508del-NBD1. BIA is located between the α/β and the α subdomains and is involved in hydrogen bond and π-cation interactions with binding site residues. The main H-bond interaction is formed between the indole hydrogen of BIA and the backbone oxygen of V562 and is maintained throughout 76% of the simulation. This interaction likely stabilizes the 551−557 region, which is highly fluctuating in all F508del-containing constructs, to roughly the wt level. R516 interacts via a π-cation interaction and a salt bridge with the indole and the acid moiety of BIA, respectively. These interactions are maintained throughout 48% and 61% of the simulation. These interactions lock the side chain of R516, therefore preventing it from forming transient interactions with residues in the 508 region. Such interactions are observed in the simulations of all F508del-containing constructs. As a result, residues in the vicinity of F508 which were found to be highly fluctuating in all F508del-containing constructs in comparison with the wt (e.g., 501−505 in F508del and 510−512 in F508del and F508del/V510D) are stabilized to roughly the wt level.

Similar to the effect exerted by the rescuing mutations, a comparison of RMSF profiles between F508del and F508del/BIA-NBD1 (Figure 8A and 8C) demonstrates an attenuation of the fluctuations at multiple regions in NBD1 (394−396, 439−444, 455−471, 474−479, 487−491, 502−507, 536−538, 556−562, 568−573, 601−603, 617−621, 640−642) to wt levels. Some of these regions (e.g., 556−562, 568−573) are in close vicinity to BIA, while others are spread all over the protein, stressing once more the high degree of allostericity within NBD1. As found for the Teem mutations, many of these regions are intercorrelated (394−396 with 439−444, 455−471 with 601−603 and with 617−621, 487−491 with 568−573, 502−507 with 556−562, 568−573 with 601−603; see red circles in Figure 9). Interestingly, nine of the residues on this list (M469, E474, L475, F490, C491, L507, S557, R560, A561) are found to be in close contact with ICL4 based on the recent CFTR model published by Mornon,[64] suggesting that the stabilization of these regions may improve the folding of the full length protein. This hypothesis is in agreement with recent results obtained by Riordan's lab which demonstrated that BIA indeed increases the maturation of F508del-CFTR.[32] Among all the perturbations considered in this work, BIA attenuates the fluctuation of F508del-NBD1 to the highest degree, yet it provides only a modest effect on the protein stability (an increase in Tm of 1.4 °C). This apparent discrepancy could be rationalized by the fact that BIA is not a strong binder of NBD1 (biacore affinity of 0.3mM only; SGX, unpublished results) and consequently spends only part of the time bound to the protein. However, this ligand maintained its position in the binding site throughout the entire length of our simulations.

The attenuation of fluctuations exerted by BIA is also observed when comparing RMSF profiles of wt and F508del/BIA-NBD1. Most of the regions found to be consistently fluctuating in F508del in comparison with wt, disappear upon complexation with BIA (501−505, 510−512, 551−557, 564−566 and 593−595), leaving only two regions (493−497 and 585−588). Two new regions emerge upon complexation with BIA, namely, 452−454 and 612−615, both in the α/β subdomain (see Figures 8B and 8D). These emerging regions appeared also in the presence of the Teem mutations and are coupled in both constructs. Thus, only 11% of the residues in F508del/BIA consistently fluctuate to a higher degree than the

DOI: 10.1021/acs.jcim.5b00312
J. Chem. Inf. Model. 2015, 55, 2349−2364

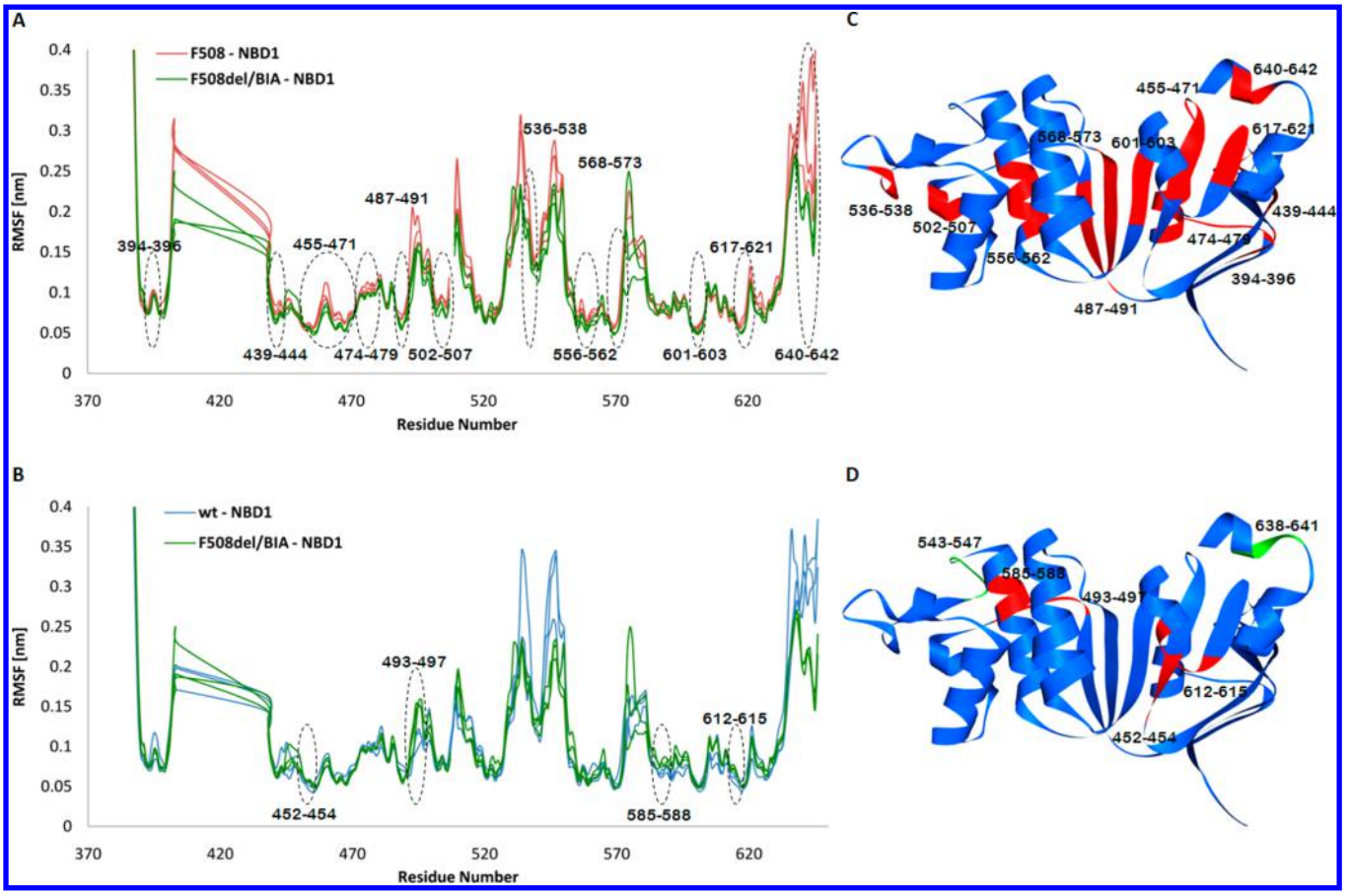

Figure 8. A comparison between RMSF profiles of wt, F508del, and F508del/BIA-NBD1 constructs from REMD simulations. (A) REMD-derived RMSF profiles for F508del (red, three repeats) and F508del/BIA-NBD1 (green, three repeats) Tm values: 51.5 and 52.9 °C for F508del and F508del/BIA-NBD1, respectively. (B) REMD-derived RMSF profiles for wt (blue, three repeats) and F508del/BIA-NBD1 (green, three repeats). Tm values: 57.7 and 52.9 °C for wt and F508del/BIA-NBD1, respectively. (C) Differences between F508del-NBD1 and F508del/BIA-NBD1 mapped on the NBD1 structure. Regions consisting of at least three consecutive residues for which F508del RMSF values are consistently higher than those of F508del/BIA are colored in red. (D) Differences between wt and F508del/BIA-NBD1 mapped on the NBD1 structure. Regions consisting of at least three consecutive residues for which F508del/BIA RMSF values are consistently higher than those of wt are colored in red. Regions consisting of at least three consecutive residues for which wt RMSF values are consistently higher than those of F508del/BIA are colored in green.

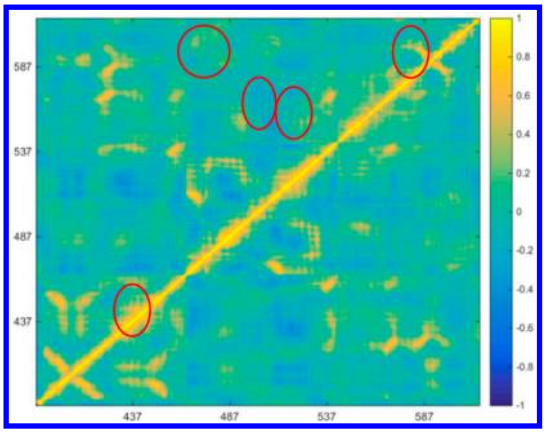

Figure 9. Correlation matrix for F508del/BIA-NBD1. Averaged covariance matrix indicating the degree of linear dependence between the movements of C_α atoms of F508del-NBD1 in the presence of BIA. Coloring scheme ranges from yellow (perfect correlation) to blue (perfect anticorrelation). Circles highlight regions discussed in the text.

corresponding residues in the wt protein, whereas 7% of the residues show an opposite behavior (Figure 8B).

3.5. Correlation between Tm and RMSF. Figure 10 presents a correlation between Tm and RMSF values (averaged over all trajectories and residues) for all seven constructs considered in this work (wt, V510D, 3M, F508del, F508del/V510D, F508del/3M, and F508del/BIA). As expected, RMSF values decrease with the increase in stability. A high correlation (R^2 = 0.82) was observed for six constructs, excluding F508del/BIA. The correlation dropped to R^2 = 0.61 upon inclusion of this construct. This decrease could be rationalized, as suggested above, by the smaller actual residence time of BIA within the binding site compared to what is observed during the simulation. Nevertheless, this correlation suggests that REMD simulations may be a viable tool for the study of the relative stability of NBD1 constructs.

3.6. Comparison between the Potential Energy Surfaces of the Different Constructs. To compare the potential energy surfaces (PESs) sampled by the different constructs, 2100 conformations from all trajectories were divided into 40 clusters as described in the Methods section. The distribution of structures from all constructs across the clusters is presented in Table 1.

DOI: 10.1021/acs.jcim.5b00312
J. Chem. Inf. Model. 2015, 55, 2349−2364

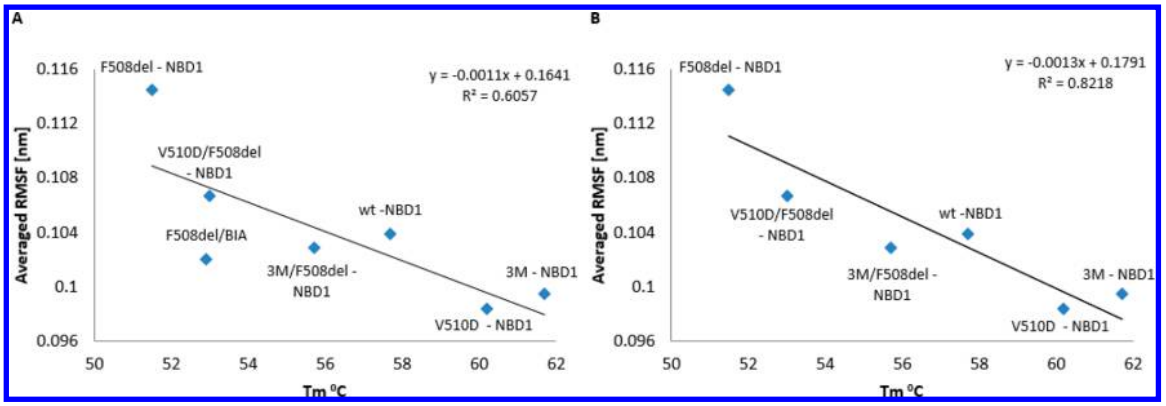

Figure 10. Correlation between Tm and RMSF values. (A) Including F508del/BIA and (B) excluding F508del/BIA.

Table 1. Cluster Analysis of 2100 NBD1 Conformations (100 Conformations for Each of the Three Repeats of the Seven Constructs Considered in This Work)[a]

cluster size	wt-NBD1	F508del-NBD1	V510D-NBD1	V510D/F508del-NBD1	3M-NBD1	3M/F508del-NBD1	F508del/BIA
1595	242	189	237	229	262	208	228
200		69	7	28	6	56	34
78		7	3	20		29	19
63	14	9	36	4			
35	4		3		28		
26	26						
21		3		8			10
6		5	1				
6			5	1			
6				6			
5						5	
5							5
4	4						
4		4					
4		2			1	1	
3	3						
3		3					
3		3					
3			3				
3					3		
2	2						
2	2						
2	2						
2		2					
2		2					
2			2				
2			1	1			
2				2			
2				1	1		
2					1	1	
2							2
1	2	2	2	1			2

[a]Clusters are ordered according to size. Entries indicate the number of conformations from each construct in each of the 40 clusters.

About 96% (2018) of all structures populate the seven largest clusters ($n \geq 21$), whereas the rest populate smaller clusters or singletons. The majority of structures (1595; 76%) populate a single cluster with similar contributions (12%−16%) from all constructs. Thus, to a first approximation, all constructs sample similar PESs. However, analyzing smaller clusters leads to some interesting observations: (1) Different constructs populate different number of clusters. Thus, F508del populates the largest number of clusters (13) in agreement with its highest fluctuation profile, wt, V510D and V510D/F508del populate intermediate numbers (10, 11, and 11, respectively) and 3M, 3M/F508del, and F508del/BIA populate the smallest numbers (7, 6, and 7, respectively). These numbers correlate ($r^2 = 0.83$) with the number of structures populating small ($n \leq 6$) clusters (15, 23, 14, 12, 6, 7, and 9, for wt, F508del, V510D, V510D/F508del, 3M, 3M/F508del, and F508del/BIA, respectively). (2) Several clusters present distinctively nonuniform population patterns. For example, the second largest cluster (200

DOI: 10.1021/acs.jcim.5b00312
J. Chem. Inf. Model. 2015, 55, 2349−2364

Table 2. Cluster Analysis of 2100 ATP Conformations (100 Conformations for Each of the Three Repeats of the Seven Constructs Considered in This Work)[a]

cluster size	wt-NBD1	F508del-NBD1	V510D-NBD1	V510D/F508del-NBD1	3M-NBD1	3M/F508del-NBD1	F508del/BIA
360	31	72	21	59	30	102	45
334	13	51	1	82	20	61	106
323	92	27	125	9	33	29	8
174	87	4	58	1	20	3	1
128	32	3	74		18		1
118	1	29		25	3	27	33
78	12	13	2	15	4	20	12
53		17		15	5	1	15
45	2	18		6		15	4
43		3		14	1	3	22
32	8	2	13	1		6	2
31		1			30		
26	4	8	1	2	6	3	2
22					22		
20		4		8	8		
20					12	1	7
17		4		2	1	7	3
15			1		14		
14		1		6		1	6
13	1	7		2	1	1	1
11		11					
11		1		10			
11				2	9		
11					8		3
10		2	1	3		3	1
9				9			
9					9		
8	1			7			
7		4		1		2	
6		3		3			
6				4	1		1
5	2	2	1				
5				3	2		
5					5		
5					2	3	
5						3	2
4	3			1			
4					4		
4					4		
4					2	2	
3	3						
3	3						
3	2	1					
3		1			2		
3					3		
3					3		
3						2	1
2	1	1					
2		2					
2		2					
2		2					
2			2				
2				2			
2				2			
2				2			
2				2			
2				1	1		
2					2		
2					2		
2					2		

DOI: 10.1021/acs.jcim.5b00312
J. Chem. Inf. Model. 2015, 55, 2349−2364

Table 2. continued

cluster size	wt-NBD1	F508del-NBD1	V510D-NBD1	V510D/F508del-NBD1	3M-NBD1	3M/F508del-NBD1	F508del/BIA
2					2		
2					1	1	
2						1	1
2							2
2							2
2							2
2							2
2							2
2							2
2							2
2							2
2							2
1	3	4		2	10	3	5

[a]Clusters are ordered according to size. Entries indicate the number of conformations from each construct in each of the 99 clusters.

conformations) is highly populated by all constructs bearing the F508del mutation but significantly less by "wt-like" constructs. This observation also holds true for the third largest cluster (78 conformations) except that this cluster is only mildly populated by the F508del mutant. Interestingly, both clusters are completely lacking conformations from the wt construct. Thus, despite their overall similarity there are some notable differences between the PESs sampled by the different constructs.

3.7. Comparison between the ATP Binding Modes in the Different Constructs. Table S3 summarizes the hydrogen bonding patterns between ATP and its neighboring residues during the REMD simulations of all constructs (see Figure S12 for the numbering system of ATP), and Table 2 presents the results of the cluster analysis performed on the 2100 ATP structures sampled during the simulations.

In all constructs the ATP maintains a similar number of hydrogen bonds with the protein (10 ± 1, 9 ± 1, 10 ± 1, 9 ± 1, 8 ± 2, 9 ± 1, and 11 ± 1 for wt-NBD1, F508del-NBD1, V510D-NBD1, V510D/F508del-NBD1, 3M-NBD1, 3M/F508del-NBD1, and F508del/BIA, respectively) primarily through its triphosphate moiety, yet these bonds are formed with different binding site residues. The resulting conformational diversity is reflected in the large number of clusters (99) populated by the different constructs. A second contribution to cluster population comes from the conformational freedom of the solvent exposed ribose and adenine rings. Overall, there is a large overlap between the ATP binding modes in the different constructs, yet there is some tendency of different constructs to populate different binding modes.

Finally, we calculated the nonbonded energies between ATP and all NBD1 constructs considered in this work. The results are presented in Table 3 and demonstrate that overall, these values are lower for wt constructs than for F508del constructs.

Table 3. Nonbonded Energies between ATP and NBD1 Averaged over All REMD Repeats for All Constructs Considered in This Work

construct	nonbonded interactions (kcal/mol)
wt-NBD1	-148 ± 17
F508del-NBD1	-113 ± 12
V510D-NBD1	-154 ± 13
V510D/F508del-NBD1	-104 ± 12
3M-NBD1	-114 ± 21
3M/F508del-NBD1	-110 ± 10
F508del/BIA	-107 ± 10

4. DISCUSSION

In this work we present the results of REMD simulations for a series of wt and F508del-NBD1 constructs. These simulations demonstrated reproducible differences in the dynamic profiles of the studied constructs, which are consistent with experimental thermal stability data.[24,31] Furthermore, we present for the first time the simulation of F508del-NBD1 in complex with a known stabilizer, BIA.

All the molecular dynamics simulations performed in this work utilized the replica exchange mechanism which was demonstrated to provide better sampling of the potential energy surface than standard MD simulations.[69] Simulations were performed within a temperature range of 300 K−349.38 K (26.85 °C−76.23 °C), higher than the melting temperatures of all constructs, and each of the 32 replicas was run for 10 ns. Each simulation was repeated three times. Thus, each construct was simulated for the equivalent of $(32 \times 10 \times 3) \approx 1$ μs. The different simulations resulted in similar RMSD values with respect to the initial structure (Figures S8−S11) and displayed very similar trends of RMSF profiles (Figures 2, 4, 5, and 8). Furthermore, the data in Table S1 and Figures S1−S7 suggest that all replicas spanned the entire temperature range making multiple transitions between different temperatures and that in all cases replicas spanning the entire temperature range contributed to the analyzed trajectory. We therefore believe that these simulations are sufficiently converged.

All simulations described in this work were initiated from the most recent crystal structures available for human NBDs from CFTR, namely, 2PZE and 2PZF. These structures do not contain any solubilizing mutations but are missing the entire RI (residues 405−436). DMD simulations have demonstrated allosteric coupling between the RI and other NBD1 subdomains.[45] However, simulations of NBD1 constructs in the presence of the RI are potentially flawed by large uncertainties in its precise structure. Indeed, the structure of the RI is known to be highly disordered and consequently was not observed in any of the available crystal structures of human NBD1. While it is difficult to compare the degree of uncertainty introduced by the complete removal of the RI with that introduced by modeling it in a potentially erroneous conformation, we opt for the first option since it allowed us to directly compare the results of our simulations with high quality thermodynamic data.[24,31] Furthermore, due to the

DOI: 10.1021/acs.jcim.5b00312
J. Chem. Inf. Model. 2015, 55, 2349−2364

improved biochemical behavior of RIdel constructs, we expect that additional data could be obtained with relative ease allowing for additional validation of our computational approach.

In contrast with the highly localized differences between wt and F508del-NBD1 observed by analyzing the static crystal structures of these proteins,[40] REMD simulations suggest that differences in their biochemical properties result from both local and nonlocal differences in their dynamic profile, which together form a dynamically coupled network. Indeed these two constructs sample somewhat different potential energy surfaces as evident from the results of the cluster analysis (see Table 1). The simulations of wt and F508del-NBD1 reveal that the F508del mutation significantly increases the fluctuations of 61 residues (28%), whereas only two residues demonstrated the opposite effect. These enhanced fluctuations correlate with the reduced thermal stability of the mutant.[24] Furthermore, this correlation extends also to constructs containing V510D, the Teem mutations, and the BIA ligand (Figures 10A and 10B).

The larger fluctuations observed for F508del-NBD1 may affect both its thermodynamic stability and the maturation and function of F508del-CFTR in several ways: (i) by increasing the aggregation tendency of the mutant domain.[24,60] For example, exposure of hydrophobic residues such as W496 and V510 could promote aggregation and aberrant intermolecular interactions; (ii) by reducing the tendency of the mutant to bind ATP,[61,62] due to the enhanced flexibility of the 491−497 region which forms part of the ATP binding site; and (iii) by impairing the interaction of F508del-NBD1 with other CFTR domains. In particular, the enhanced fluctuations in regions 501−505 and 510−512 may compromise the interactions between this domain and the coupling helix which forms part of ICL4, interactions which are believed to be critical for the maturation of the full length protein.[27,28] Furthermore, due to the deletion of F508, W496 changes its conformation and forms a hydrogen bond with E543 which may therefore be partially prevented from forming important contacts with ICL3 and ICL4. Finally, residue 501 was assumed to participate in NBD1-ICL1 interactions.[41] Larger fluctuations of this residue, as found in our analysis, may result in weaker binding of NBD1 to ICL1.

A comparison between RMSF profiles of F508del constructs in the presence of suppressor mutations and between RMSF profiles of wt and F508del-NBD1 may help to elucidate the mechanism by which these mutations exert their stabilizing effect. The suppressor mutations reduce the fluctuations of multiple (sometimes intercorrelated) regions within NBD1, both in their vicinity and in remote regions, highlighting the high degree of allostericity of NBD1. In doing so they bring the RMSF profiles of the corresponding constructs closer to that of wt. Thus, 28% of the residues in the parent F508del-NBD1 construct show enhanced flexibility compared with the wt construct. This percentage is reduced to 17% and 14% in the presence of V510D and the Teem mutations, respectively, in accord with the higher thermal stability induced by the latter mutations (V510D and the Teem mutations increase the thermal stability of F508del-NBD1 by 1.5° and 4.2°, respectively). A closer scrutiny of the data reveals that two highly fluctuating regions in F508del-NBD1, 501−505, and 564−566 disappear upon inclusion of either of the suppressor mutations, suggesting that the stabilization of these regions is important for the thermal stability of the constructs and possibly for rescuing F508del-CFTR. The overall stabilization, induced by the different rescuing mutations, reduced the RMSF profiles of the corresponding constructs toward wt levels. Moreover, inspection of a recently published CFTR model suggests that specific regions stabilized by either rescuing mutation form contacts with ICL3 (499−502 and 539−542 stabilized by 3M) and ICL4 (467−473 and 487−490 stabilized by V510D). Stabilization of these regions may therefore promote the maturation of mutant CFTR.

The stabilizing effect of suppressor mutations (e.g., Teem mutations,[25] deletion of RI,[45] and introduction of Proline residues[70]) on the background of wt and F508del-NBD1 and the resulting (albeit partial) translation of this effect to the maturation of F508del-CFTR supports a model by which the F508del mutation affects some inherent properties of NBD1 itself, thereby suggesting that F508del-NBD1 is a viable target for F508del-CFTR rescuing. Indeed, Odolczyk et al. have recently reported the discovery of a new F508del-CFTR corrector that targets NBD1,[71] and He et al. have demonstrated that restoring the thermal stability of NBD1 is sufficient to promote F508del-CFTR maturation.[32] However, studies from the Thomas and Lukacs laboratories suggest that rescuing F508del-CFTR to wt levels requires correcting both the inherent defect of F508del-NBD1 as well as its interactions with other CFTR domains, in particular ICL4, and therefore support a "combination of correctors" therapy to CF with different ligands stabilizing NBD1 itself and, e.g., the NBD1-MSD1/MSD2 interface.[27,28] However, a single ligand, like BIA, may fulfill both requirements, as it strongly attenuates the overall RMSF profile of F508del/BIA bringing it to wt levels (translated into a 1.4° increase in Tm) and at the same time it specifically stabilizes regions which are known to be in contact with ICL1 and ICL4 (e.g., 501−505 and 510−512).

Regions 501−505 and 564−566 are stabilized to wt levels by both BIA and the V510D and 3M mutations. These regions may therefore be important for the stabilization of NBD1. In contrast, residues 493−497 and 588 maintain consistently higher fluctuation levels (in comparison with wt) in all F508del-containing constructs. We therefore hypothesize that stabilization of these regions will further stabilize F508del-NBD1.

Taken together the data presented in this work suggest that REMD simulations are useful for predicting relative stabilities of NBD1 constructs and for elucidating the mechanism of action of rescuing mutations and NBD1 binders. Such simulations could also be useful for drug design, elucidating ligand-NBD1 binding interactions in a time-dependent manner and suggesting potency-increasing modifications prior to synthesis. Moreover, we have recently demonstrated the binding of a dual acting CFTR modulator (CFFT-001) to a binding site located at the C-terminus of F508del, RIdel, and REdel-NBD1. Interestingly, this binding site was not observed in the relevant crystal structures but was clearly apparent from the analysis of REMD-generated trajectories.[72] This suggests that an analysis of similar trajectories obtained in the present work may reveal additional sites which could be used for the discovery of multiple NBD1 modulators.

As a proof of concept, we have subjected one of the F508del REMD trajectories to a pocket searching procedure using the MDpocket algorithm (see the Methods section for more details). Figure 11 presents the binding sites found to be conserved during the simulation and their volumes. This analysis points to potential drugable sites on F508del which could be targeted by future virtual screening campaigns.

DOI: 10.1021/acs.jcim.5b00312
J. Chem. Inf. Model. 2015, 55, 2349−2364

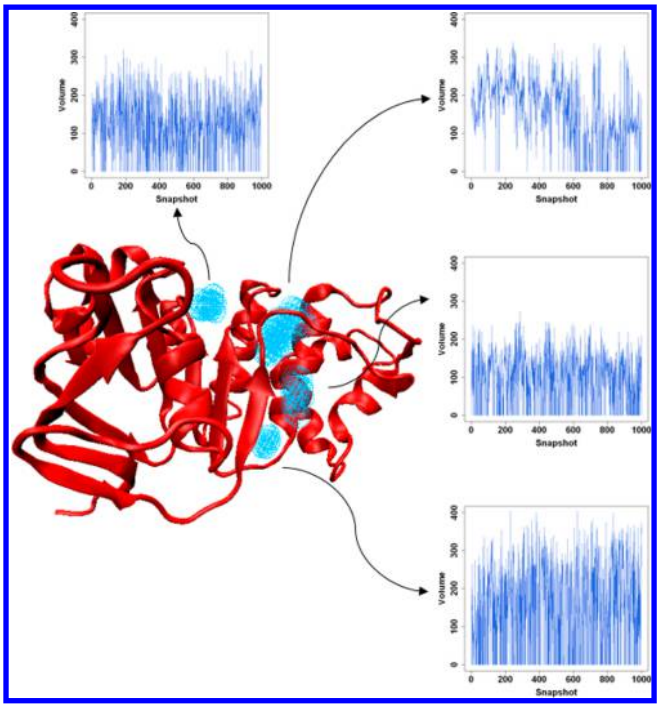

Figure 11. Four binding sites (in blue) conserved throughout a representative REMD simulation of F508del-NBD1. Inserts show the volume (Å^3) of each site during the simulation.

Finally, experimental and computational studies of protein folding and unfolding have suggested a connection between early unfolding events and atomic fluctuations showing that the most flexible atoms are generally the first to unfold.[73−76] Thus, the highly fluctuating regions identified in the mutant protein may be "unfolding-prone" and consequently plausible candidates for stabilization via mutational and/or pharmaceutical intervention.

5. CONCLUSIONS

This work presents the results of multiple REMD simulations on seven NBD1 constructs from human CFTR, the main protein implicated in Cystic Fibrosis, including its wt form, its most common CF-causing mutation (F508del), both wt and F508del mutant in the presence of rescuing mutations (V510D and the Teem mutations), and F508del-NBD1 in the presence of a known NBD1 stabilizer, the BIA ligand. The resulting REMD-generated RMSF profiles were shown to correlate with thermal stabilities of the different constructs, to be sensitive to small changes at the sequence level (e.g., the introduction of single mutations), to provide insight into their structural and energetic consequences, and to unveil the mechanism by which they exert their deleterious (F508del), rescuing (V510D, Teem), and stabilizing (BIA) effects. In addition, these simulations demonstrate the existence of a complex network of allosteric interactions which spreads across the entire protein and which couples protein regions both local to and distant from the F508del mutation. Taken together, these results suggest that REMD simulations are an efficient tool for analyzing the properties of CFTR domains which cannot be revealed only by examining static crystal structures. Importantly, this type of analysis could be extended to study the effect of CFTR modulators targeting NBD1 once reliable experimental information on their putative binding sites becomes available. While the present work focuses on specific mutations in NBD1 from human CFTR, Nucleotide Binding Domains (NBDs) are found in many other proteins and moreover, in some cases (e.g., P-glycoprotein), mutations in these domains analogous to F508del, lead to similar folding problems. Thus, the work described in this study could be extended to the study of other mutations both in NBD1 from human CFTR and to NBDs of other proteins.

■ ASSOCIATED CONTENT

Supporting Information

The Supporting Information is available free of charge on the ACS Publications website at DOI: 10.1021/acs.jcim.5b00312.

Figures S1−S12 and Tables S1−S3 (PDF)

■ AUTHOR INFORMATION

Corresponding Author

*E-mail: hsenderowitz@gmail.com.

Notes

The authors declare no competing financial interest.

■ ACKNOWLEDGMENTS

This work was supported by the Cystic Fibrosis Foundation, grant No. SENDER09XX0. We would like to thank J. Spencer Emtage, Hal A Lewis, Shane Atwell, and the entire SGX Pharmaceutical CFTR team for providing the unpublished crystal coordinates data for the BIA complex with NBD1.

■ REFERENCES

(1) Cheung, J. C.; Deber, C. M. Misfolding of the Cystic Fibrosis Transmembrane Conductance Regulator and Disease. *Biochemistry* **2008**, *47*, 1465−1473.

(2) Bompadre, S. G.; Hwang, T. C. Cystic Fibrosis Transmembrane Conductance Regulator: A Chloride Channel Gated by ATP Binding and Hydrolysis. *ShengLi XueBao* **2007**, *59*, 431−442.

(3) Gadsby, D. C.; Vergani, P.; Csanady, L. The ABC Protein Turned Chloride Channel Whose Failure Causes Cystic Fibrosis. *Nature* **2006**, *440*, 477−483.

(4) Sheppard, D. N.; Welsh, M. J. Structure and Function of the CFTR Chloride Channel. *Physiol. Rev.* **1999**, *79*, S23−45.

(5) Csanady, L.; Nairn, A. C.; Gadsby, D. C. Thermodynamics of CFTR Channel Gating: A Spreading Conformational Change Initiates an Irreversible Gating Cycle. *J. Gen. Physiol.* **2006**, *128*, 523−533.

(6) Mense, M.; Vergani, P.; White, D. M.; Altberg, G.; Nairn, A. C.; Gadsby, D. C. In Vivo Phosphorylation of CFTR Promotes Formation of a Nucleotide-Binding Domain Heterodimer. *EMBO J.* **2006**, *25*, 4728−4739.

(7) Vergani, P.; Basso, C.; Mense, M.; Nairn, A. C.; Gadsby, D. C. Control of the CFTR Channel's Gates. *Biochem. Soc. Trans.* **2005**, *33*, 1003−1007.

(8) Vergani, P.; Lockless, S. W.; Nairn, A. C.; Gadsby, D. C. CFTR Channel Opening by ATP-Driven Tight Dimerization of Its Nucleotide-Binding Domains. *Nature* **2005**, *433*, 876−880.

(9) Mornon, J. P.; Lehn, P.; Callebaut, I. Molecular Models of the Open and Closed States of the Whole Human CFTR Protein. *Cell. Mol. Life Sci.* **2009**, *66*, 3469−3486.

(10) Baker, J. M. R.; Hudson, R. P.; Kanelis, V.; Choy, W.-Y.; Thibodeau, P. H.; Thomas, P. J.; Forman-Kay, J. D. CFTR Regulatory Region Interacts with NBD1 Predominantly Via Multiple Transient Helices. *Nat. Struct. Mol. Biol.* **2007**, *14*, 738−745.

(11) Cystic Fibrosis Mutation Database: http://www.genet.sickkids.on.ca/.

(12) Riordan, J. R. CFTR Function and Prospects for Therapy. *Annu. Rev. Biochem.* **2008**, *77*, 701−726.

(13) Miki, H.; Zhou, Z.; Li, M.; Hwang, T. C.; Bompadre, S. G. Potentiation of Disease-Associated Cystic Fibrosis Transmembrane

DOI: 10.1021/acs.jcim.5b00312
J. Chem. Inf. Model. 2015, 55, 2349−2364

Conductance Regulator Mutants by Hydrolyzable ATP Analogs. *J. Biol. Chem.* **2010**, *285*, 19967−19975.
(14) Gentzsch, M.; Chang, X. B.; Cui, L.; Wu, Y.; Ozols, V. V.; Choudhury, A.; Pagano, R. E.; Riordan, J. R. Endocytic Trafficking Routes of Wild Type and DeltaF508 Cystic Fibrosis Transmembrane Conductance Regulator. *Mol. Biol. Cell* **2004**, *15*, 2684−2696.
(15) Lukacs, G. L.; Chang, X. B.; Bear, C.; Kartner, N.; Mohamed, A.; Riordan, J. R.; Grinstein, S. The Delta F508 Mutation Decreases the Stability of Cystic Fibrosis Transmembrane Conductance Regulator in the Plasma Membrane. Determination of Functional Half-Lives on Transfected Cells. *J. Biol. Chem.* **1993**, *268*, 21592−21598.
(16) Swiatecka-Urban, A.; Brown, A.; Moreau-Marquis, S.; Renuka, J.; Coutermarsh, B.; Barnaby, R.; Karlson, K. H.; Flotte, T. R.; Fukuda, M.; Langford, G. M.; Stanton, B. A. The Short Apical Membrane Half-Life of Rescued {Delta}F508-Cystic Fibrosis Transmembrane Conductance Regulator (CFTR) Results from Accelerated Endocytosis of {Delta}F508-CFTR in Polarized Human Airway Epithelial Cells. *J. Biol. Chem.* **2005**, *280*, 36762−36772.
(17) Lukacs, G. L.; Verkman, A. S. CFTR: Folding, Misfolding and Correcting the DeltaF508 Conformational Defect. *Trends Mol. Med.* **2012**, *18*, 81−91.
(18) Chen, E. Y.; Bartlett, M. C.; Loo, T. W.; Clarke, D. M. The DeltaF508 Mutation Disrupts Packing of the Transmembrane Segments of the Cystic Fibrosis Transmembrane Conductance Regulator. *J. Biol. Chem.* **2004**, *279*, 39620−39627.
(19) Cyr, D. M. Arrest of CFTR DeltaF508 Folding. *Nat. Struct. Mol. Biol.* **2005**, *12*, 2−3.
(20) Du, K.; Sharma, M.; Lukacs, G. L. The DeltaF508 Cystic Fibrosis Mutation Impairs Domain-Domain Interactions and Arrests Post-Translational Folding of CFTR. *Nat. Struct. Mol. Biol.* **2005**, *12*, 17−25.
(21) Thibodeau, P. H.; Brautigam, C. A.; Machius, M.; Thomas, P. J. Side Chain and Backbone Contributions of Phe508 to CFTR Folding. *Nat. Struct. Mol. Biol.* **2005**, *12*, 10−16.
(22) Cui, L.; Aleksandrov, L.; Chang, X. B.; Hou, Y. X.; He, L.; Hegedus, T.; Gentzsch, M.; Aleksandrov, A.; Balch, W. E.; Riordan, J. R. Domain Interdependence in the Biosynthetic Assembly of CFTR. *J. Mol. Biol.* **2007**, *365*, 981−994.
(23) Rosser, M. F.; Grove, D. E.; Chen, L.; Cyr, D. M. Assembly and Misassembly of Cystic Fibrosis Transmembrane Conductance Regulator: Folding Defects Caused by Deletion of F508 Occur before and after the Calnexin-Dependent Association of Membrane Spanning Domain (MSD) 1 and MSD2. *Mol. Biol. Cell* **2008**, *19*, 4570−4579.
(24) Protasevich, I.; Yang, Z.; Wang, C.; Atwell, S.; Zhao, X.; Emtage, S.; Wetmore, D.; Hunt, J. F.; Brouillette, C. G. Thermal Unfolding Studies Show the Disease Causing F508del Mutation in CFTR Thermodynamically Destabilizes Nucleotide-Binding Domain 1. *Protein Sci.* **2010**, *19*, 1917−1931.
(25) Thibodeau, P. H.; Richardson, J. M., 3rd; Wang, W.; Millen, L.; Watson, J.; Mendoza, J. L.; Du, K.; Fischman, S.; Senderowitz, H.; Lukacs, G. L.; Kirk, K.; Thomas, P. J. The Cystic Fibrosis-Causing Mutation DeltaF508 Affects Multiple Steps in Cystic Fibrosis Transmembrane Conductance Regulator Biogenesis. *J. Biol. Chem.* **2010**, *285*, 35825−35835.
(26) He, L.; Aleksandrov, L. A.; Cui, L.; Jensen, T. J.; Nesbitt, K. L.; Riordan, J. R. Restoration of Domain Folding and Interdomain Assembly by Second-Site Suppressors of the DeltaF508 Mutation in CFTR. *FASEB J.* **2010**, *24*, 3103−3112.
(27) Mendoza, J. L.; Schmidt, A.; Li, Q.; Nuvaga, E.; Barrett, T.; Bridges, R. J.; Feranchak, A. P.; Brautigam, C. A.; Thomas, P. J. Requirements for Efficient Correction of DeltaF508 CFTR Revealed by Analyses of Evolved Sequences. *Cell* **2012**, *148*, 164−174.
(28) Rabeh, W. M.; Bossard, F.; Xu, H.; Okiyoneda, T.; Bagdany, M.; Mulvihill, C. M.; Du, K.; di Bernardo, S.; Liu, Y.; Konermann, L.; Roldan, A.; Lukacs, G. L. Correction of Both NBD1 Energetics and Domain Interface Is Required to Restore DeltaF508 CFTR Folding and Function. *Cell* **2012**, *148*, 150−163.
(29) Wang, Y.; Loo, T. W.; Bartlett, M. C.; Clarke, D. M. Correctors Promote Maturation of Cystic Fibrosis Transmembrane Conductance Regulator (CFTR)-Processing Mutants by Binding to the Protein. *J. Biol. Chem.* **2007**, *282*, 33247−33251.
(30) Loo, T. W.; Bartlett, M. C.; Clarke, D. M. The V510D Suppressor Mutation Stabilizes DeltaF508-CFTR at the Cell Surface. *Biochemistry* **2010**, *49*, 6352−6357.
(31) Wang, C.; Protasevich, I.; Yang, Z.; Seehausen, D.; Skalak, T.; Zhao, X.; Atwell, S.; Spencer Emtage, J.; Wetmore, D. R.; Brouillette, C. G.; Hunt, J. F. Integrated Biophysical Studies Implicate Partial Unfolding of NBD1 of CFTR in the Molecular Pathogenesis of F508del Cystic Fibrosis. *Protein Sci.* **2010**, *19*, 1932−1947.
(32) He, L.; Aleksandrov, A. A.; An, J.; Cui, L.; Yang, Z.; Brouillette, C. G.; Riordan, J. R. Restoration of NBD1 Thermal Stability Is Necessary and Sufficient to Correct ΔF508 CFTR Folding and Assembly. *J. Mol. Biol.* **2015**, *427*, 106−120.
(33) Van Goor, F.; Hadida, S.; Grootenhuis, P. D.; Burton, B.; Cao, D.; Neuberger, T.; Turnbull, A.; Singh, A.; Joubran, J.; Hazlewood, A.; Zhou, J.; McCartney, J.; Arumugam, V.; Decker, C.; Yang, J.; Young, C.; Olson, E. R.; Wine, J. J.; Frizzell, R. A.; Ashlock, M.; Negulescu, P. Rescue of CF Airway Epithelial Cell Function in Vitro by a CFTR Potentiator, VX-770. *Proc. Natl. Acad. Sci. U. S. A.* **2009**, *106*, 18825−18830.
(34) Yu, H.; Burton, B.; Huang, C. J.; Worley, J.; Cao, D.; Johnson, J. P., Jr.; Urrutia, A.; Joubran, J.; Seepersaud, S.; Sussky, K.; Hoffman, B. J.; Van Goor, F. Ivacaftor Potentiation of Multiple CFTR Channels with Gating Mutations. *J. Cystic Fibrosis* **2012**, *11*, 237−245.
(35) Ren, H. Y.; Grove, D. E.; De La Rosa, O.; Houck, S. A.; Sopha, P.; Van Goor, F.; Hoffman, B. J.; Cyr, D. M. VX-809 Corrects Folding Defects in Cystic Fibrosis Transmembrane Conductance Regulator Protein through Action on Membrane-Spanning Domain 1. *Mol. Biol. Cell* **2013**, *24*, 3016−3024.
(36) Atwell, S.; Brouillette, C. G.; Conners, K.; Emtage, S.; Gheyi, T.; Guggino, W. B.; Hendle, J.; Hunt, J. F.; Lewis, H. A.; Lu, F.; Protasevich, II; Rodgers, L. A.; Romero, R.; Wasserman, S. R.; Weber, P. C.; Wetmore, D.; Zhang, F. F.; Zhao, X. Structures of a Minimal Human CFTR First Nucleotide-Binding Domain as a Monomer, Head-to-Tail Homodimer, and Pathogenic Mutant. *Protein Eng., Des. Sel.* **2010**, *23*, 375−384.
(37) Atwell, S.; Conners, K.; Emtage, S.; Gheyi, T.; Lewis, H.; Lu, F.; Romero, R.; Zhao, X. Structure of the Human CFTR NBD1 Domain as a Homodimer: Insights and Applications. *Pediatric Pulmonology* **2007**, 100−101.
(38) Lewis, H. A.; Buchanan, S. G.; Burley, S. K.; Conners, K.; Dickey, M.; Dorwart, M.; Fowler, R.; Gao, X.; Guggino, W. B.; Hendrickson, W. A.; Hunt, J. F.; Kearins, M. C.; Lorimer, D.; Maloney, P. C.; Post, K. W.; Rajashankar, K. R.; Rutter, M. E.; Sauder, J. M.; Shriver, S.; Thibodeau, P. H.; Thomas, P. J.; Zhang, M.; Zhao, X.; Emtage, S. Structure of Nucleotide-Binding Domain 1 of the Cystic Fibrosis Transmembrane Conductance Regulator. *EMBO J.* **2004**, *23*, 282−293.
(39) Moody, J. E.; Millen, L.; Binns, D.; Hunt, J. F.; Thomas, P. J. Cooperative, ATP-Dependent Association of the Nucleotide Binding Cassettes During the Catalytic Cycle of ATP-Binding Cassette Transporters. *J. Biol. Chem.* **2002**, *277*, 21111−21114.
(40) Lewis, H. A.; Wang, C.; Zhao, X.; Hamuro, Y.; Conners, K.; Kearins, M. C.; Lu, F.; Sauder, J. M.; Molnar, K. S.; Coales, S. J.; Maloney, P. C.; Guggino, W. B.; Wetmore, D. R.; Weber, P. C.; Hunt, J. F. Structure and Dynamics of NBD1 from CFTR Characterized Using Crystallography and Hydrogen/Deuterium Exchange Mass Spectrometry. *J. Mol. Biol.* **2010**, *396*, 406−430.
(41) Kanelis, V.; Hudson, R. P.; Thibodeau, P. H.; Thomas, P. J.; Forman-Kay, J. D. NMR Evidence for Differential Phosphorylation-Dependent Interactions in Wt and DeltaF508 CFTR. *EMBO J.* **2010**, *29*, 263−277.
(42) Wieczorek, G.; Zielenkiewicz, P. DeltaF508 Mutation Increases Conformational Flexibility of CFTR Protein. *J. Cystic Fibrosis* **2008**, *7*, 295−300.
(43) Bisignano, P.; Moran, O. Molecular Dynamics Analysis of the Wild Type and DF508 Mutant Structures of the Human CFTR-Nucleotide Binding Domain 1. *Biochimie* **2010**, *92*, 51−57.

DOI: 10.1021/acs.jcim.5b00312
J. Chem. Inf. Model. 2015, 55, 2349−2364

(44) Proctor, E. A.; Kota, P.; Aleksandrov, A. A.; He, L.; Riordan, J. R.; Dokholyan, N. V. Rational Coupled Dynamics Network Manipulation Rescues Disease-Relevant Mutant Cystic Fibrosis Transmembrane Conductance Regulator. *Chem. Sci.* **2015**, *6*, 1237−1246.
(45) Aleksandrov, A. A.; Kota, P.; Aleksandrov, L. A.; He, L.; Jensen, T.; Cui, L.; Gentzsch, M.; Dokholyan, N. V.; Riordan, J. R. Regulatory Insertion Removal Restores Maturation, Stability and Function of DeltaF508 CFTR. *J. Mol. Biol.* **2010**, *401*, 194−210.
(46) Accelrys *Discovery Studio Modeling Environment*, 2.5; Accelrys Software Inc.: San Diego, 2005−2009.
(47) Schrodinger *Maestro*, 9.0; Schrodinger: NY, 2009.
(48) Berendsen, H. J. C.; van der Spoel, D.; van Drunen, R. Gromacs: A Message-Passing Parallel Molecular Dynamics Implementation. *Comput. Phys. Commun.* **1995**, *91*, 43−56.
(49) Hess, B.; Kutzner, C.; van der Spoel, D.; Lindahl, E. Gromacs 4: Algorithms for Highly Efficient, Load-Balanced, and Scalable Molecular Simulation. *J. Chem. Theory Comput.* **2008**, *4*, 435−447.
(50) Kaminski, G. A.; Friesner, R. A.; Tirado-Rives, J.; Jorgensen, W. L. Evaluation and Reparametrization of the OPLS-AA Force Field for Proteins Via Comparison with Accurate Quantum Chemical Calculations on Peptides. *J. Phys. Chem. B* **2001**, *105*, 6474−6487.
(51) Berendsen, H. J. C.; Postma, J. P. M.; Vangunsteren, W. F.; Dinola, A.; Haak, J. R. Molecular-Dynamics with Coupling to an External Bath. *J. Chem. Phys.* **1984**, *81*, 3684−3690.
(52) Hockney, R. W.; Goel, S. P.; Eastwood, J. W. Quiet High-Resolution Computer Models of a Plasma. *J. Comput. Phys.* **1974**, *14*, 148−158.
(53) Darden, T.; York, D.; Pedersen, L. Particle Mesh Ewald - an N.Log(N) Method for Ewald Sums in Large Systems. *J. Chem. Phys.* **1993**, *98*, 10089−10092.
(54) Essmann, U.; Perera, L.; Berkowitz, M. L.; Darden, T.; Lee, H.; Pedersen, L. G. A Smooth Particle Mesh Ewald Method. *J. Chem. Phys.* **1995**, *103*, 8577−8593.
(55) Hess, B.; Bekker, H.; Berendsen, H.; Fraaije, J. Lincs: A Linear Constraint Solver for Molecular Simulations. *J. Comput. Chem.* **1997**, *18*, 1463−1472.
(56) Patriksson, A.; van der Spoel, D. A Temperature Predictor for Parallel Tempering Simulations. *Phys. Chem. Chem. Phys.* **2008**, *10*, 2073−2077.
(57) Eisenhaber, F.; Lijnzaad, P.; Argos, P.; Sander, C.; Scharf, M. The Double Cubic Lattice Method: Efficient Approaches to Numerical Integration of Surface Area and Volume and to Dot Surface Contouring of Molecular Assemblies. *J. Comput. Chem.* **1995**, *16*, 273−284.
(58) Sharma, S.; Ding, F.; Dokholyan, N. V. Multiscale Modeling of Nucleosome Dynamics. *Biophys. J.* **2007**, *92*, 1457−1470.
(59) Schmidtke, P.; Bidon-Chanal, A.; Luque, F. J.; Barril, X. Mdpocket: Open-Source Cavity Detection and Characterization on Molecular Dynamics Trajectories. *Bioinformatics* **2011**, *27*, 3276−3285.
(60) Hoelen, H.; Kleizen, B.; Schmidt, A.; Richardson, J.; Charitou, P.; Thomas, P. J.; Braakman, I. The Primary Folding Defect and Rescue of DeltaF508 CFTR Emerge During Translation of the Mutant Domain. *PLoS One* **2010**, *5*, e15458.
(61) Haws, C. M.; Nepomuceno, I. B.; Krouse, M. E.; Wakelee, H.; Law, T.; Xia, Y.; Nguyen, H.; Wine, J. J. Delta F508-CFTR Channels: Kinetics, Activation by Forskolin, and Potentiation by Xanthines. *Am. J. Physiol.* **1996**, *270*, C1544−1555.
(62) Wellhauser, L.; Kim Chiaw, P.; Pasyk, S.; Li, C.; Ramjeesingh, M.; Bear, C. E. A Small-Molecule Modulator Interacts Directly with Deltaphe508-CFTR to Modify Its ATPase Activity and Conformational Stability. *Mol. Pharmacol.* **2009**, *75*, 1430−1438.
(63) He, L.; Aleksandrov, A. A.; Serohijos, A. W.; Hegedus, T.; Aleksandrov, L. A.; Cui, L.; Dokholyan, N. V.; Riordan, J. R. Multiple Membrane-Cytoplasmic Domain Contacts in the Cystic Fibrosis Transmembrane Conductance Regulator (CFTR) Mediate Regulation of Channel Gating. *J. Biol. Chem.* **2008**, *283*, 26383−26390.
(64) Mornon, J.-P.; Hoffmann, B.; Jonic, S.; Lehn, P.; Callebaut, I. Full-Open and Closed CFTR Channels, with Lateral Tunnels from the Cytoplasm and an Alternative Position of the F508 Region, as Revealed by Molecular Dynamics. *Cell. Mol. Life Sci.* **2015**, *72*, 1377−1403.
(65) Kumar, S.; Nussinov, R. Salt Bridge Stability in Monomeric Proteins. *J. Mol. Biol.* **1999**, *293*, 1241−1255.
(66) DeCarvalho, A. C.; Gansheroff, L. J.; Teem, J. L. Mutations in the Nucleotide Binding Domain 1 Signature Motif Region Rescue Processing and Functional Defects of Cystic Fibrosis Transmembrane Conductance Regulator Delta F508. *J. Biol. Chem.* **2002**, *277*, 35896−35905.
(67) Teem, J. L.; Berger, H. A.; Ostedgaard, L. S.; Rich, D. P.; Tsui, L. C.; Welsh, M. J. Identification of Revertants for the Cystic Fibrosis Delta F508 Mutation Using Ste6-CFTR Chimeras in Yeast. *Cell* **1993**, *73*, 335−346.
(68) Teem, J. L.; Carson, M. R.; Welsh, M. J. Mutation of R555 in CFTR-Delta F508 Enhances Function and Partially Corrects Defective Processing. *Recept. Channels* **1996**, *4*, 63−72.
(69) Sugita, Y.; Okamoto, Y. Replica-Exchange Molecular Dynamics Method for Protein Folding. *Chem. Phys. Lett.* **1999**, *314*, 141−151.
(70) Aleksandrov, A. A.; Kota, P.; Cui, L.; Jensen, T.; Alekseev, A. E.; Reyes, S.; He, L.; Gentzsch, M.; Aleksandrov, L. A.; Dokholyan, N. V.; Riordan, J. R. Allosteric Modulation Balances Thermodynamic Stability and Restores Function of DeltaF508 CFTR. *J. Mol. Biol.* **2012**, *419*, 41−60.
(71) Odolczyk, N.; Fritsch, J.; Norez, C.; Servel, N.; da Cunha, M. F.; Bitam, S.; Kupniewska, A.; Wiszniewski, L.; Colas, J.; Tarnowski, K.; Tondelier, D.; Roldan, A.; Saussereau, E. L.; Melin-Heschel, P.; Wieczorek, G.; Lukacs, G. L.; Dadlez, M.; Faure, G.; Herrmann, H.; Ollero, M.; Becq, F.; Zielenkiewicz, P.; Edelman, A. Discovery of Novel Potent ΔF508-CFTR Correctors That Target the Nucleotide Binding Domain. *EMBO Mol. Med.* **2013**, *5*, 1484−1501.
(72) Hudson, R. P.; Chong, P. A.; Protasevich, II; Vernon, R.; Noy, E.; Bihler, H.; An, J. L.; Kalid, O.; Sela-Culang, I.; Mense, M.; Senderowitz, H.; Brouillette, C. G.; Forman-Kay, J. D. Conformational Changes Relevant to Channel Activity and Folding within the First Nucleotide Binding Domain of the Cystic Fibrosis Transmembrane Conductance Regulator. *J. Biol. Chem.* **2012**, *287*, 28480−28494.
(73) Benson, N. C.; Daggett, V. Dynameomics: Large-Scale Assessment of Native Protein Flexibility. *Protein Sci.* **2008**, *17*, 2038−2050.
(74) Fersht, A. R.; Daggett, V. Protein Folding and Unfolding at Atomic Resolution. *Cell* **2002**, *108*, 573−582.
(75) Schaeffer, R. D.; Daggett, V. Protein Folds and Protein Folding. *Protein Eng., Des. Sel.* **2011**, *24*, 11−19.
(76) van der Kamp, M. W.; Schaeffer, R. D.; Jonsson, A. L.; Scouras, A. D.; Simms, A. M.; Toofanny, R. D.; Benson, N. C.; Anderson, P. C.; Merkley, E. D.; Rysavy, S.; Bromley, D.; Beck, D. A. C.; Daggett, V. Dynameomics: A Comprehensive Database of Protein Dynamics. *Structure* **2010**, *18*, 423−435.

DOI: 10.1021/acs.jcim.5b00312
J. Chem. Inf. Model. 2015, 55, 2349−2364